ELM destabilization by externally applied non-axisymmetric magnetic perturbations in NSTX

2010 Nucl. Fusion 50 034012

(http://iopscience.iop.org/0029-5515/50/3/034012)

Nucl. Fusion **50** (2010) 034012 (8pp) doi:10.1088/0029-5515/50/3/034012

ELM destabilization by externally applied non-axisymmetric magnetic perturbations in NSTX

J.M. Canik[1,a], R. Maingi[1], T.E. Evans[2], R.E. Bell[3], S.P. Gerhardt[3], H.W. Kugel[3], B.P. LeBlanc[3], J. Manickam[3], J.E. Menard[3], T.H. Osborne[2], J.-K. Park[3], S. Paul[3], P.B. Snyder[2], S.A. Sabbagh[4], E.A. Unterberg[5] and the NSTX team

[1] Oak Ridge National Laboratory, Oak Ridge, TN 37831, USA
[2] General Atomics, San Diego, CA 92186, USA
[3] Princeton Plasma Physics Laboratory, Princeton, NJ 08543, USA
[4] Columbia University, New York, NY 10027, USA
[5] Oak Ridge Institute for Science and Education, Oak Ridge, TN 37831, USA

E-mail: canikjm@ornl.gov

Received 15 May 2009, accepted for publication 15 December 2009
Published 23 February 2010
Online at stacks.iop.org/NF/50/034012

Abstract
We report on a recent set of experiments performed in NSTX to explore the effects of non-axisymmetric magnetic perturbations on the stability of edge-localized modes (ELMs). The application of these 3D fields in NSTX was found to have a strong effect on ELM stability, including the destabilization of ELMs in H-modes otherwise free of large ELMs. Exploiting the effect of the perturbations, ELMs have been controllably introduced into lithium-enhanced ELM-free H-modes, causing a reduction in impurity accumulation while maintaining high confinement. Although these experiments show the principle of the combined use of lithium coatings and 3D fields, further optimization is required in order to reduce the size of the induced ELMs.

PACS numbers: 52.55.Fa

(Some figures in this article are in colour only in the electronic version)

1. Introduction

Edge-localized modes (ELMs) produce periodic expulsions of energy and particles during H-mode operation of tokamaks [1]. Although the rapid energy loss during an ELM poses a threat to the lifetime of plasma-facing components due to erosion, the presence of ELMs has the clear benefit of increasing impurity transport [2]. In the absence of ELMs, impurity buildup is often observed, making the ELM-free H-mode a transient operational scenario unless a mechanism can be found for increasing impurity transport (as seen in the QH [3], EDA [4] and RMP H-modes [5]). The accumulation of impurities in the absence of ELMs becomes especially important in spherical tori, where it has been predicted that, due to the strong shaping and low aspect ratio, extremely high pedestal pressures may be achieved before ELM stability limits are reached [6]. If realized, this high pedestal pressure limit scenario could lead to a situation in which global stability limits are reached before ELM onset, and operation could be naturally limited to the ELM-free H-mode. Indeed, recent experiments in NSTX have shown such a situation arising when the plasma-facing components are coated with lithium; in these discharges ELMs are completely suppressed, and the energy confinement is significantly improved [7–9]. Not surprisingly, these plasmas also show strong impurity accumulation.

Here we report on a recent set of experiments performed in NSTX in which non-axisymmetric magnetic perturbations have been utilized to control the impurity buildup. The use of non-axisymmetric fields with a strong resonant component (resonant magnetic perturbations—RMPs) has been proposed as a method to mitigate or suppress ELMs by reducing the pedestal pressure gradient; this technique has been successfully demonstrated on the DIII-D [5] and JET [10] tokamaks, and coils are being designed to employ this ELM control method on ITER. The application of RMPs in NSTX was found to have a strong effect on ELM stability, including the destabilization of ELMs in H-modes otherwise free of large ELMs. A similar transformation from ELM-free to ELMy

[a] Author to whom any correspondence should be addressed.

H-mode has been previously observed on COMPASS-D [11] and JFT-2M [12], and more recently in the MAST spherical tokamak, where initial experiments exploring the effects of $n = 3$ RMPs have shown the destabilization of type-III ELMs [13]. Exploiting this effect of the RMPs in NSTX, ELMs have been controllably introduced into lithium-enhanced ELM-free H-modes, causing a reduction in impurity accumulation while maintaining high confinement.

NSTX is a low aspect ratio device, with a major radius of 0.85 m and a minor radius of 0.65 m. In the experiments described here, the toroidal magnetic field and plasma current were fixed at 0.45 T and 800 kA, respectively, and the plasma was heated with up to 6 MW of neutral beam injection. The perturbation fields are generated by a set of six midplane coils that are typically used for error field correction and resistive wall mode feedback control [14]. These coils are external, but close-fitting to the vacuum vessel. In the ELM destabilization experiments these have been configured to apply an $n = 3$ field, and, as discussed in section 3, produce a largely non-resonant perturbation, with still significant resonant components.

2. Experimental observations of ELM destabilization with applied 3D magnetic fields

In the initial ELM destabilization experiments, lithium coatings of the wall were not used. The plasmas studied had double null boundary shapes with $\delta_r^{sep} \sim 0$ (δ_r^{sep} is the radial distance between the upper and lower divertor separatrices, measured at the outboard midplane), with moderate elongation of $\kappa = 2.0$ and high triangularity $\delta = 0.7$. The neutral beam heating power in these plasmas was 6 MW. Under these conditions, the plasma discharges are characterized by a relatively long period free of large ELMs (very small type V ELMs [15] are generally present in NSTX discharges without lithium conditioning). This can be seen in figure 1, which shows time traces of stored energy, line-average density, and lower divertor D_α emission from a reference discharge where no RMP is applied (solid lines). As can be seen from the D_α traces in panel (*d*), the discharge is free of large ELMs from $t \sim 0.3$ to 0.5 s.

In the second discharge shown in figure 1 (dashed lines), the RMP is applied from $t = 0.35$ to 0.45 s; see the midplane coil currents shown in panel (*e*). This time corresponds to the large-ELM-free phase in the reference discharge. As the D_α traces in panel (*e*) show, ELMs begin within 50 ms of the application of the RMP. The typical size of these ELMs is $\Delta W / W_{tot} \sim 3$–5% (here ΔW is the drop in stored energy due to a single ELM and W_{tot} is the stored energy before the ELM). After a short ELMy period, the RMP was removed, and the plasma returned to an ELM-free (or small-ELM) state. At $t = 0.55$ s, another 100 ms long pulse of the RMP was imposed, and again large ELMs began shortly after the RMP was turned on and ceased when it was removed. Thus, ELM stability is closely linked to the presence of the perturbed fields, and does not appear to be simply due to a change in the discharge evolution causing an earlier end to the ELM-free phase.

Figure 2 shows the D_α emission from a series of discharges in which the magnitude of the RMP was varied to determine the applied field threshold for destabilization. Panel (*a*) shows that at 900 A of current in the midplane coil set (corresponding

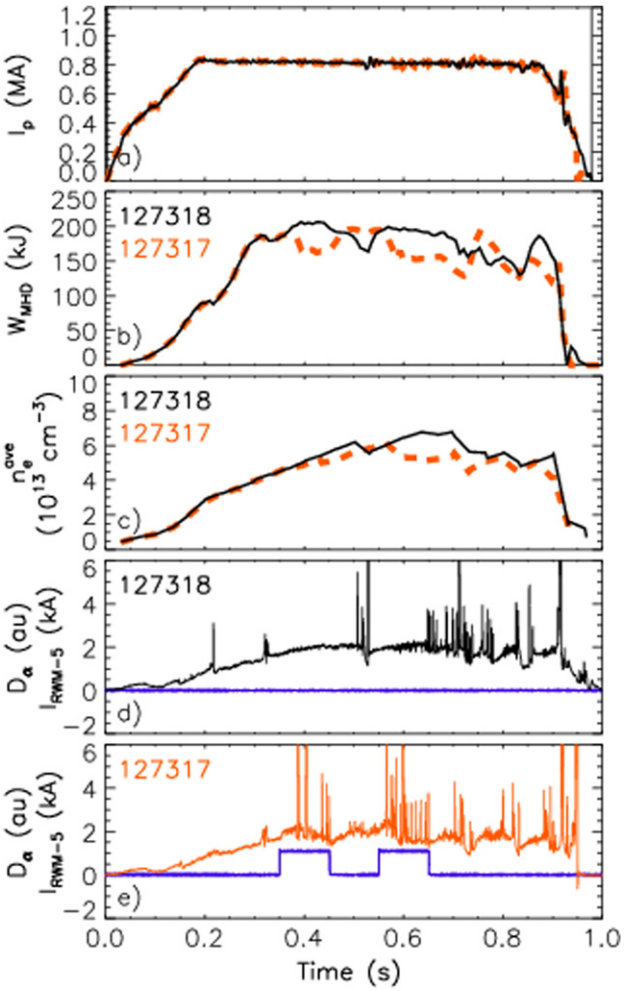

Figure 1. Time evolution of (*a*) plasma current, (*b*) stored energy and (*c*) line-average density in a reference discharge (solid black line) and a discharge with RMP applied (dashed line). Traces of lower divertor D_α emission and current in the midplane coil set in (*d*) the reference discharge, and (*e*) in the discharge with RMP.

to $\Delta B/B_t \sim 6 \times 10^{-3}$ at the top of the pedestal), the RMP does not have a clear effect on ELM stability; ELMs begin at $t \sim 0.5$ s, which corresponds to the end of the natural ELM-free phase. At 0.95 and 1.0 kA, ELMs are clearly triggered, but are intermittent, showing behaviour that might be expected near the threshold for destabilization. At the highest current shown, 1.3 kA, a series of regular ELMs are triggered. Although the ELM onset is somewhat later in panel (*d*), where the $n = 3$ application is delayed compared with the discharges shown in panels (*b*) and (*c*), this trend does not persist in other discharges; the variability in the ELM onset time is not understood. The data from this limited range of currents indicate that the ELM frequency increases with the perturbation level above the threshold for destabilization. However, the highest current levels strongly brake plasma rotation and degrade stability [14], so that global instabilities arise shortly (typically ~100 ms) after the RMP is applied, which make the apparent increase in ELM frequency with perturbation level difficult to verify.

Profiles of the electron density, n_e, electron and ion temperatures, T_e and T_i, and toroidal rotation are shown in

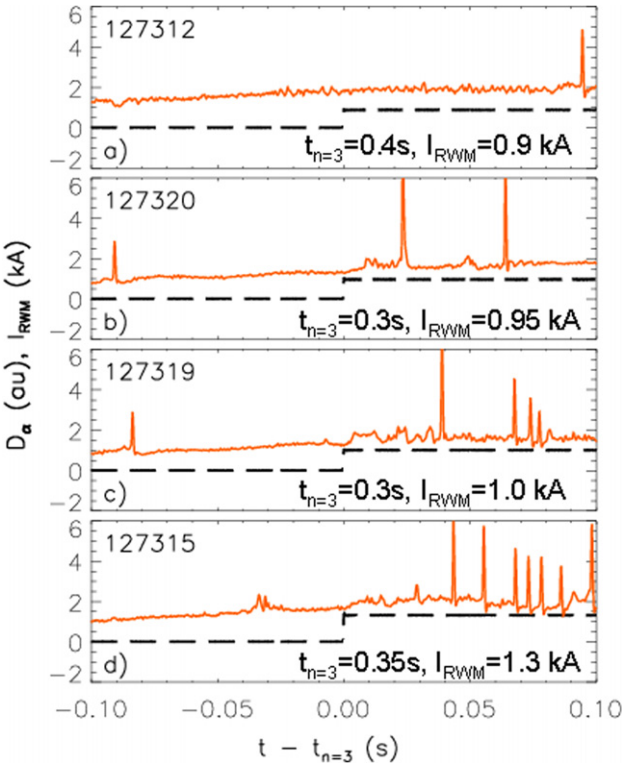

Figure 2. Current in the midplane coil set and D_α emission from a series of discharges in which the perturbation magnitude was varied.

figure 3. These are taken at time of $t \sim 0.37$ s into the discharges shown in figure 1; this time point is 20 ms after the RMP is applied in shot 127317, and 20 ms before the first ELM occurs. As the figure shows, the core profiles of the density and temperatures are essentially unchanged with RMP application as compared with the reference discharge. The clearest change is in the toroidal rotation, which is reduced significantly across the plasma radius when the $n = 3$ field is applied; this is qualitatively consistent with the rotational braking due to neoclassical toroidal viscosity (NTV) that has previously been observed on NSTX when non-axisymmetric fields are applied [16]. In addition to the change in rotation, the pedestal electron temperature T_e shows an increase when the RMP is applied; this is visible at the most inboard point of the profile. This change is consistent across several discharges in which the $n = 3$ field is applied, and is most clear when mapped into poloidal flux (panel (*e*)). The ion temperature is relatively unchanged when the perturbation is applied, so that the total edge pressure gradient increases by ∼30% in the pedestal, based on fitting of the profiles to a modified tanh function [17]; this may be responsible for the change in ELM stability when the $n = 3$ field is applied.

Calculations using the PEST MHD stability code [18] using these experimental profiles show that the pedestal is stable before the $n = 3$ field is applied and is unstable to low n (∼2–4) edge modes after the field is applied. Peeling–ballooning stability has also been evaluated with the ELITE code [19], and shows that with the $n = 3$ field applied the pedestal lies near the peeling instability boundary, although the growth rates are significantly less than those calculated with PEST. These results are in contrast to experiments where resonant fields are used to suppress ELMs [10, 20] where a reduction in the pedestal density is observed, and the reduced pressure gradient leads to improved stability consistent with peeling–ballooning calculations [21].

3. Characteristics of the magnetic perturbations

The spectrum of the dominant $n = 3$ part of the applied perturbation is shown in figure 4; this spectrum represents the normal component of the vacuum perturbation with no plasma response included, using the PEST coordinate system [22]. The single row of midplane coils creates a largely non-resonant magnetic field, with the spectrum peaking at low poloidal mode number, especially in the core (figure 4(*a*)). However, since the coils are relatively short compared with the plasma (the coils extend 1 m in the vertical direction, whereas the plasma height is typically 2.5 m in these experiments), the spectrum extends to high poloidal mode numbers towards the periphery of the plasma. Due to this, the perturbation contains strong resonant components in this region. This can be seen in figure 4(*b*)), where the poloidal spectra are shown for radii of 0.85, 0.9 and 0.95, with the mode number resonant with the q profile highlighted (note that these are not rational surfaces, but are simply chosen to illustrate the poloidal spectrum). Although these resonant terms have led to the use of the term 'RMP', it is not known whether the resonant or non-resonant components play a dominant role in the destabilization of ELMs.

Using the vacuum perturbation, the spectrum is used to calculate the island width at rational surfaces, and the corresponding Chirikov parameter [23] ($\sigma_{CH} > 1$ indicates overlapping islands and the onset of stochasticity). This parameter is useful as a measure of the effectiveness of the resonant field components in forming a stochastic layer. From the vacuum approximation, the magnetic field is stochastic outside a radius of $\psi_N \sim 0.6$ (figure 4(*c*)), which is a significantly wider stochastic layer than has empirically been found to be necessary for the suppression of ELMs at DIII-D [24] (although it should be noted that significant differences exist in these experiments, including the shape, aspect ratio, magnetic shear and notably the collisionality: $\nu^*_{ped} \sim 2$–3 in the NSTX experiments, roughly an order of magnitude higher than those described in [24]).

The wide stochastic layer in the vacuum approximation (a superposition of the 2D equilibrium magnetic fields with the vacuum perturbation, again with no plasma response included) is confirmed by field line tracing, as seen in the Poincare plot shown in figure 5. Here field lines are followed starting with initial values of $\psi_N = 0.1$ out to the edge in increments of 0.1. The stable and unstable manifolds [25] associated with the two X-points are also shown, illustrating the change to the separatrix topology caused by the RMP. The manifolds are calculated by following a field line originating very near the X-point for a toroidal turn, constructing a line between the starting and end points of this field line, and mapping this line segment toroidally several times, as outlined in [26]. These structures are similar to those predicted and observed in RMP experiments at DIII-D [27, 28], and can be expected to cause a splitting of the footprints of heat and particle fluxes on the divertor plates [29]. Future experiments will measure these footprints to confirm the presence of such structures.

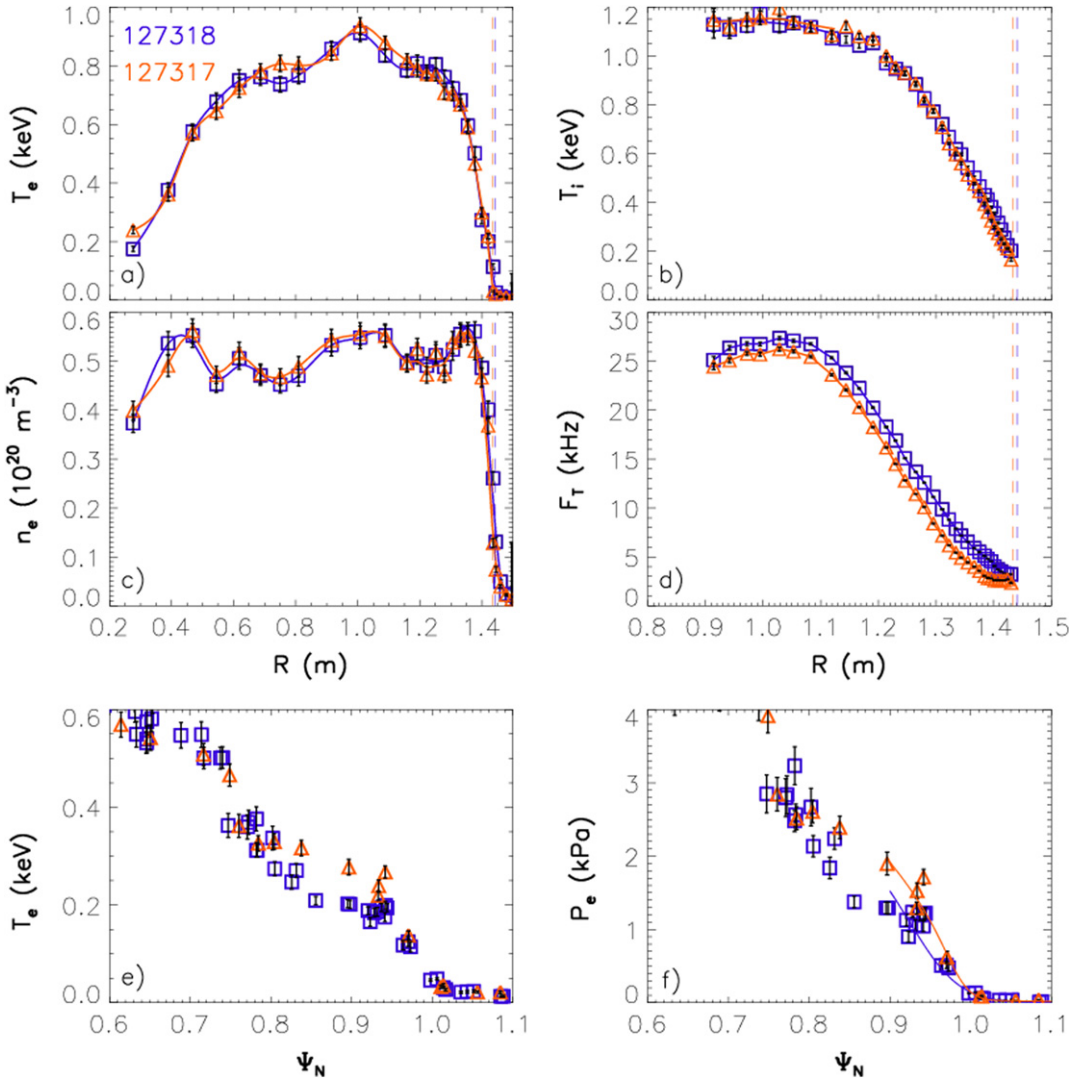

Figure 3. Profiles at $t = 0.37$ s of electron (*a*) density and (*b*) temperature, (*c*) ion temperature and (*d*) toroidal rotation frequency from the reference discharge (squares) and with RMP applied (triangles) (vertical dashed lines indicate separatrix position). Pedestal profiles of the electron (*e*) temperature and (*f*) pressure with fits to a modified tanh function.

While the lack of a strong impact on core plasma profiles is suggestive that the resonant fields have not penetrated to the core by the time at which the measurements are made (e.g. that the resonant fields are screened [30]), the RMP does have an impact on the edge profiles (figure 3). Although the measured increase in electron temperature is the opposite of the classically expected increase in transport caused by a stochastic field [31], it has been elsewhere observed that confinement can be improved in the presence of RMPs [32, 33], with the improvement attributed to changes in the radial electric field [34].

The ideal plasma response has been calculated using the IPEC code [35]. As shown in figure 4(*d*)), the Chirikov parameter based on the IPEC calculations is above unity only at the far edge of the plasma. Here, the Chirikov parameter is only used as a measure of the strength of the resonant field; in this ideal approximation, parallel currents flow at rational surfaces which shield the resonant fields and prevent islands from forming [36], and so $\sigma_{\mathrm{CH}} > 1$ in this case does not indicate stochasticity. The IPEC calculation indicates that the ideal plasma response, in addition to maintaining closed flux surfaces, attenuates the resonant field components in the plasma core. In these calculations, the non-resonant magnetic field components remain strong enough to cause a significant NTV [37], which may be the cause of the observed global reduction in toroidal rotation.

4. ELM pace-making in lithium enhanced ELM-free H-modes

The use of lithium coatings on plasma-facing components has been shown to markedly reduce hydrogen recycling, leading to enhanced density evolution control [38, 39]. Recently, it has been demonstrated on NSTX that lithium conditioning of the plasma-facing components has a strong impact on plasma performance. Lithium is deposited via a pair of toroidal displaced evaporators that are opened to the vessel between shots. With lithium coatings, two major changes to the plasma are observed: an improvement in the energy confinement, primarily through the electron channel [8], and

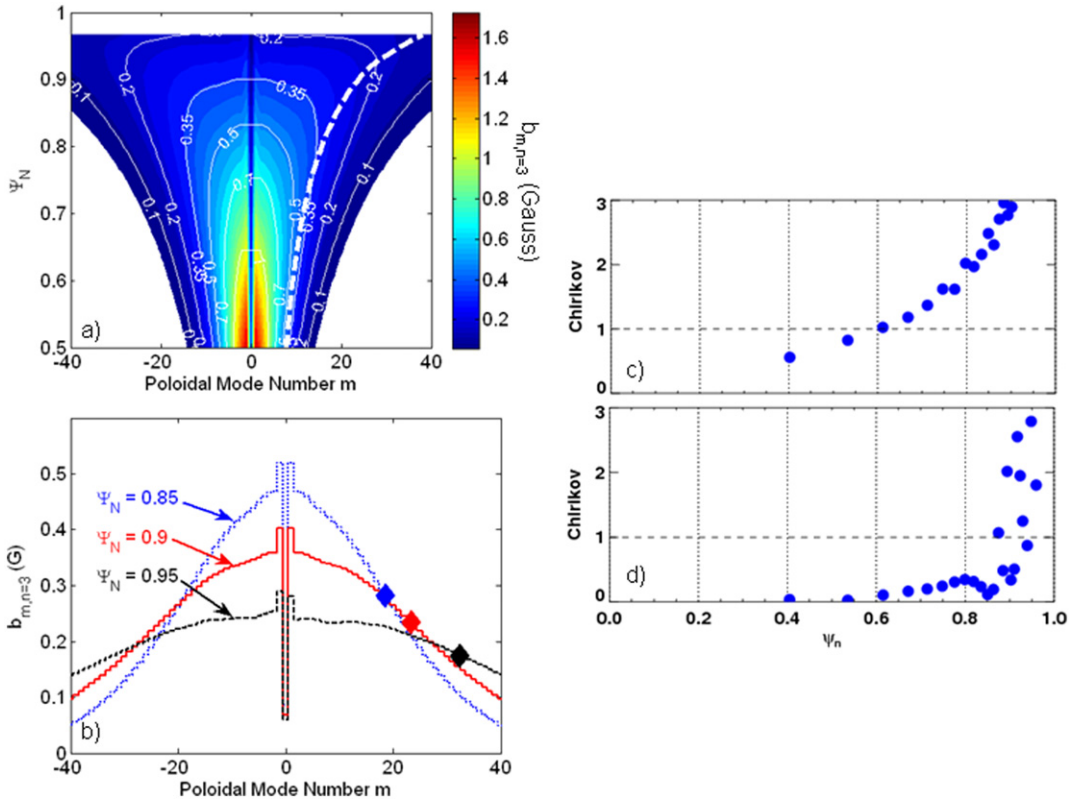

Figure 4. Poloidal spectrum of $n = 3$ perturbation (a) over a range of radial range, with the value resonant with q shown as white dashed line; (b) for three flux surfaces, with resonant values shown as diamonds; Chirikov parameter due to $n = 3$ perturbation calculated using (c) vacuum magnetic perturbation and with (d) IPEC.

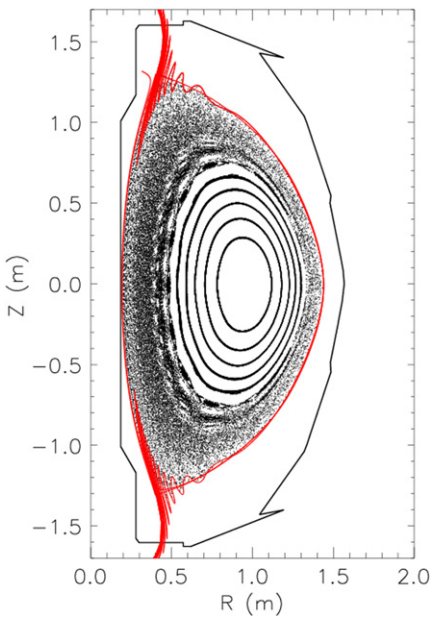

Figure 5. Poincare plot of field line structure using a superposition of the 2D magnetic fields with the vacuum perturbation. Also shown are the stable and unstable manifolds associated with the X-points.

the complete suppression of ELMs [9]. An example of such a discharge can be seen in figure 6, where the black curves show a reference discharge with lithium conditioned walls. This discharge again has a double null boundary shape with $\delta_r^{sep} \sim 0$ and a triangularity of $\delta = 0.7$, but has a higher elongation than the plasmas discussed in the previous section, with $\kappa = 2.4$. The neutral beam heating power in this plasma was 3 MW. Although the results with lithium conditioning show great promise for improving overall performance, the plasmas also exhibit the non-stationary nature typical of the ELM-free H-mode: the particle transport is in effect too low, so that the density and impurity content increase throughout the discharge, eventually leading to a radiative collapse. This can be seen in panel (e) of figure 6, where in the reference discharge the radiated power increases to ∼1.5 MW near the end of the discharge, while panel (f) shows that the edge Z_{eff} reaches a value of ∼5.

In order to reduce the density and impurity accumulation, experiments were performed in which RMP was used to controllably introduce ELMs into discharges with lithium wall conditioning, with the goal of gaining the particle control advantages of the ELMs, while retaining the high energy confinement seen with lithium. Figure 6 (pale lines) shows the time traces from a discharge in which the RMP was applied to trigger ELMs. In this case, the fields were applied in the form of a pulse train, with 11 ms pulses being applied at a frequency of 40 Hz. This waveform was chosen to minimize the duty cycle of the RMP, and reduces the time-averaged impact on plasma rotation and stability. As seen in the D_α traces in panel (c), the applied RMP successfully destabilize ELMs, with ∼75% of the pulses triggering an ELM. Before the pulses begin, and hence before any ELMs are triggered, the density and radiated power evolution are similar to the reference discharge. Once the ELMs start, however, the rate

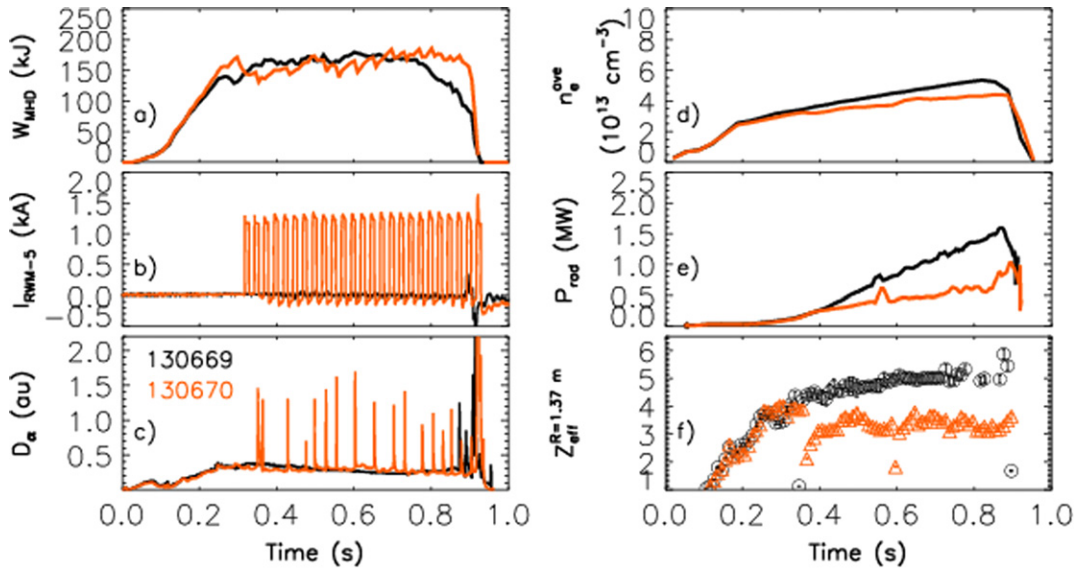

Figure 6. Time traces of (*a*) stored energy, (*b*) current in the perturbation coil set, (*c*) D_α emission, (*d*) line-averaged density, (*e*) radiated power and (*f*) effective charge based on carbon density at $R = 1.37$ m (near the top of the pedestal) for a control discharge (black) and with pulses of RMP applied (pale solid lines).

of density rise is decreased (panel (*d*)), as is that of the radiated power (panel (*e*) and $Z_{\rm eff}$ due to carbon in the pedestal region (panel f; note that lithium does not contribute substantially to $Z_{\rm eff}$ in either case, as carbon and metallic species are the dominant impurities [40]). At a time of 0.8 s, near the end of the discharge, the density and radiation are 20% and 50% lower in the case with ELM triggering than in the control discharge, and the pedestal $Z_{\rm eff}$ is reduced by 30%. The stored energy, on the other hand, is not strongly affected in a time-averaged send (each ELM leads to a transient loss of energy), and in fact is sustained at a high value for a longer time in the discharge with RMP pulses than in the control case. This indicates that the energy confinement is similar in the two discharges, and has not been degraded by the presence of ELMs in the paced discharge.

Magnetic ELM pace-making combined with lithium conditioning has been performed in discharges with elongations in the range of $\kappa = 2$–2.55. In all cases, the benefits of the ELMs on discharge evolution are evident, as the discharges with RMP show reduced density and impurity content. In addition, it is found that at higher elongation, ELMs can be triggered more frequently by increasing the frequency of the RMP pulses; at lower κ, increasing the applied field frequency leads to unreliable triggering, so that the ELM frequency is not increased. The ELM size also shows a dependence on elongation, as shown in figure 7, with typical ELM size being smaller as κ is increased. In this figure, the average drop in the total plasma stored energy due to an ELM, $\Delta W_{\rm tot}/W$, is $\sim$ 20% for discharges with $\kappa < 2.3$. For $\kappa > 2.3$, the most probable ELM size is reduced to $\sim$3%, although large ELMs with $\Delta W_{\rm tot}/W$ greater than 10% still occur. The decrease in ELM size at high elongation may be due to the higher frequency ELM triggering that can be achieved or to a reduced ELM-affected area at the higher values of q_{95} [41].

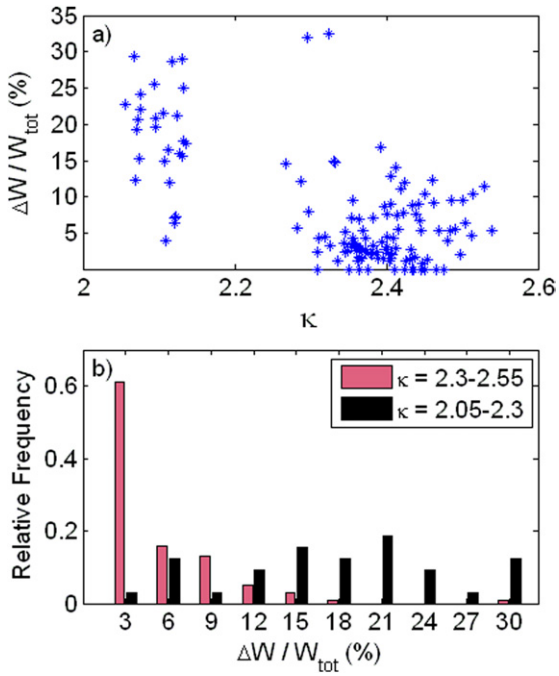

Figure 7. Dependence of the triggered ELM size on elongation: (*a*) size of each ELM versus elongation and (*b*) relative frequency of ELM sizes for low and high elongation.

5. Prospects for improved performance with combined lithium coatings and RMPs

The experiments described in the previous section demonstrate that ELM pace-making with externally applied RMPs is a viable method for reducing the density and impurity content in lithium-enhanced ELM-free H-modes. This suggests the combined use of lithium coatings to improve energy

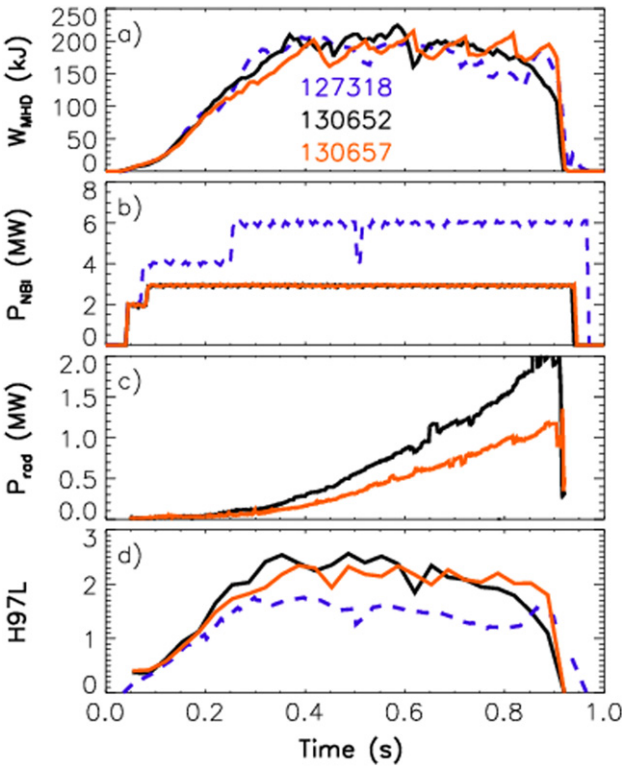

Figure 8. Time dependence of (*a*) stored energy, (*b*) neutral beam power, (*c*) radiated power and (*d*) H97L factor for a discharge with no lithium conditioning (solid black line), with lithium conditioning only (dashed line), and with combined lithium conditioning with magnetic ELM pace-making (pale solid line) The NBI waveform is the same for both discharges with lithium conditioning; the radiated power for the case with no lithium conditioning is not shown.

confinement with the application of RMPs to control the discharge evolution as a possible high-performance scenario for future operation of NSTX. Figure 8 shows time traces from the control discharge shown in figure 1, which has no lithium coatings on the walls (dashed lines), along with data from a discharge with lithium coatings but without ELM pace-making (solid black line), and finally from a discharge with combined lithium conditioning and RMPs applied to trigger ELMs (pale solid line). The plasma shape is the same in the three discharges, with an elongation of $\kappa = 2$; although ELM-pacing is less effective in this low-κ shape than the higher κ case of figure 6 (with larger triggered ELMs and less reduction in P_{rad}); it is shown here to illustrate the improvement in energy confinement of the lithium conditioning over an otherwise similar non-lithium case. All three discharges have approximately the same stored energy; however, the neutral beam power with lithium conditioning is 3 MW, compared with 6 MW without lithium. This is because with lithium conditioning, higher beam power increased β_N to 5–6, reaching the ideal limit and terminating the discharge. The improvement in confinement is quantified by the H97L factor [42] shown in panel (*d*)), which increases from ∼1.5 to nearly 2.5 when lithium coatings are applied. As was observed in the higher κ case of figure 6, the magnetic ELM-pacing does not substantially reduce the overall energy confinement, so that the discharge with combined lithium and RMP pulses shows an H-factor that remains more than 30% higher than the discharge

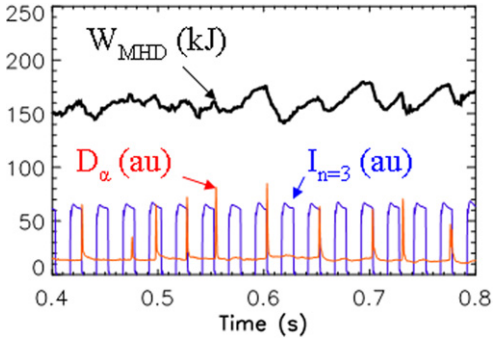

Figure 9. Time evolution of the stored energy, RMP pulses and D_α emission for the high-κ, lithium conditioned discharge of figure 6.

without lithium conditioning. The radiated power from the two lithium conditioned discharges is shown in panel (*c*). Although the radiated power is reduced by nearly a factor of two with the RMP pulses, the reduction is less pronounced than the high-κ case shown in figure 6. This is likely due to the lower frequency of the triggered ELMs achievable at this elongation; more optimization of the ELM pace-making is clearly necessary to bring the discharge to a stationary condition in this shape.

As noted in section 3, the ELMs that are destabilized by the RMP application with lithium conditioned plasma-facing components tend to be quite large, with ELM energy losses of up to 25% of the total stored plasma energy. Ideally, the ELM pace-making would make use of very small ELMs, with a frequency high enough to fully arrest the increase in density and radiated power. The decrease in the ELM size shown in figure 7 suggests one possible way to achieving small triggered ELMs, by going to higher κ. Elongation as high as $\kappa = 2.7$ have been achieved in NSTX [43], so a substantial improvement may be possible through shape optimization.

Further optimization may also be possible by improving the efficiency with which the RMPs cause ELMs. Figure 9 shows the evolution of the stored energy, D_α emission and current in the midplane coil set (bottom dark line). These traces correspond to the high κ discharge of figure 6. Note that for the RMP pulses that do not trigger an ELM, no drop in the stored energy is observed. Thus, the RMPs in themselves do not affect the plasma confinement; this is consistent with the observation that the core profiles were largely unaffected by the RMP without lithium conditioning (see figure 3). From the data shown in figure 9, the largest ELMs tend to occur after a RMP pulse has failed to produce an ELM. Thus, the ELM size may be decreased by improving the reliability of the triggering. The RMP pulses are each 11 ms in duration, and as can be seen from the spikes in the D_α light, the ELMs typically occur near the end of the RMP pulse. As might be expected, applying shorter pulses than this time that it takes to trigger an ELM results in less reliable triggering; using longer pulses, on the other hand, tends to impose too much braking of the plasma rotation and degrades global stability. The ELM-triggering time may be limited by the time it takes the externally applied perturbations to penetrate though the vacuum vessel, which is estimated to have an e-folding time of ∼4 ms. Thus, the use of internal coils to generate the RMP has the potential to considerably speed up the triggering the ELMs, which would allow higher frequency pacing for a fixed RMP duty cycle, and could therefore reduce the size of each individual ELM.

6. Discussion and conclusions

The application of non-axisymmetric magnetic fields has been observed to affect ELM stability on NSTX, causing ELMs in an otherwise small-ELM or ELM-free H-mode. When the perturbation is applied, it is observed that the toroidal rotation decreases across the plasma minor radius, and the pedestal electron temperature increases. In these experiments, the relative roles of the resonant and non-resonant terms in the spectrum of the perturbation—both of which are strong—cannot be separated. The core decrease in the toroidal rotation can be attributed to NTV caused by non-resonant perturbations, which may be altered by the ideal plasma response [36]. The RMP clearly affects the pedestal thermal profiles, although the mechanism for this effect is so far unclear; this could be related to edge electric fields and the observed change in rotation profiles, and their response to both the non-resonant and resonant fields. This will be a focus of future experiments.

Initial calculations indicate that the ELM behaviour is consistent with peeling–ballooning stability being degraded by the increased pressure gradient; however, other mechanisms for the ELM destabilization can be considered. One such mechanism is the induction of edge currents due to rapid changes in plasma position; this mechanism is attributed to the ELM triggering observed when the vertical position of the plasma is rapidly jogged [44]. However, reconstructions of the plasma equilibrium do not show evidence for substantial position oscillations caused by the RMP. This is consistent with the lack of significant $n = 0$ components in the spectrum of applied perturbation. In addition, the triggering of multiple ELMs using a quasi-steady state RMP waveform (figure 2(d)) suggests that, if edge currents are modified by the NANP, this modification is not solely caused by the rapid turn-on of the field. While changes in the edge current caused by the RMP may still be an important part of the altered ELM stability, any such changes do not appear to require rapid changes in the applied field. The ELMs could also be linked to changes to plasma current carried on open field lines, which has been conjectured to be an important part of the ELM process [45]. The invariant manifolds as shown in figure 5 could play a key role; it has been conjectured that currents flowing in flux tubes defined by these structures are responsible for the explosive growth of ELMs [46]. The existence of these structures and their possible role in the ELM behaviour will be studied in future experiments.

The triggering effect of the RMPs has been used to controllably reintroduce ELMs into lithium-enhanced ELM-free H-modes. This technique has been successful in reducing the secular increase in both the plasma density and radiated power. The discharges with magnetic ELM pace-making do not show a significant degradation of the energy confinement, and in fact show that the stored energy can sustained for a longer time. The triggered ELMs are quite large, exhausting as much as 25% of the total stored energy. However, the ELM size shows a favourable dependence on elongation, as does the achievable triggering frequency. This dependence may allow faster, smaller ELMs to be introduced at higher values of κ, which will be explored in future experiments. In addition, the ELM frequency may be substantially increased by the use of internal coils, leading to the prospect of very small-ELM size. These results demonstrate the feasibility of an operational scenario wherein lithium wall conditions are used to improve energy confinement, and magnetic ELM pace-making is employed for discharge evolution control while maintaining high performance.

Acknowledgments

This research was sponsored in part by the US Department of Energy Contracts DE-AC05-00OR22725, DE-AC02-76CH 03073, DE-FC02-04ER54698 and DE-FG02-99ER54524.

References

[1] Zohm H. 1996 *Plasma Phys. Control. Fusion* **38** 105
[2] Hill D.N. 1997 *J. Nucl. Mater.* **241–243** 182
[3] Burrell K.H. *et al* 2001 *Phys. Plamas* **8** 2153
[4] Greenwald M. *et al* 2000 *Plasma Phys. Control. Fusion* **42** A263
[5] Evans T.E. *et al* 2004 *Phys. Rev. Lett.* **92** 235003
[6] Snyder P.B. 2004 *Plasma Phys. Control. Fusion* **46** A131
[7] Maingi R. *et al* 2009 *Phys. Rev. Lett.* **103** 075001
[8] Kugel H. *et al* 2008 *Phys. Plasmas* **15** 056118
[9] Mansfield D. *et al* 2009 *J. Nucl. Mater.* **390–391** 764
[10] Liang Y. *et al* 2007 *Phys. Rev. Lett.* **98** 265004
[11] Fielding S.J. *et al* 2001 *Europhys. Conf. Abstracts* **25A** 1825
[12] Shoji T. *et al* 1992 *J. Nucl. Mater.* **196–198** 296
[13] Nardon E. *et al* 2010 *Nucl. Fusion* **49** 034002
[14] Sabbagh S.A. *et al* 2006 *Phys. Rev. Lett.* **97** 045004
[15] Maingi R. *et al* 2005 *Nucl. Fusion* **45** 264
[16] Zhu W. *et al* 2006 *Phys. Rev. Lett.* **96** 225002
[17] Groebner R.J. and Osborne T.H. 1998 *Phys. Plasmas* **5** 1800
[18] Grimm R. *et al* 1976 *Methods Comput. Phys.* **16** 253
[19] Snyder P.B. *et al* 2002 *Phys. Plasmas* **9** 2037
[20] Evans T.E. *et al* 2008 *Nucl. Fusion* **48** 024002
[21] Osborne T.H. *et al* 2008 *J. Phys. Conf. Ser.* **123** 012014
[22] Park J.-K. *et al* 2008 *Phys. Plasmas* **15** 064501
[23] Chirikov B.V. 1979 *Phys. Rep.* **52** 263
[24] Fenstermacher M.E. *et al* 2008 *Phys. Plasmas* **15** 056122
[25] Evans T.E. 2008 *Chaos, Complexity and Transport: Theory and Applications* ed C. Chandre *et al* (Singapore: World Scientific)
[26] Wingen A. *et al* 2005 *Contrib. Plasma Phys.* **45** 500
[27] Evans T. *et al* 2005 *J. Phys. Conf. Ser.* **7** 174
[28] Wingen A. *et al* 2009 *Phys. Plasmas* **16** 042504
[29] Schmitz O. *et al* 2008 *Plasma Phys. Control. Fusion* **50** 124029
[30] Fitzpatrick R. 1998 *Phys. Plasmas* **5** 3325
[31] Rechester A.B. and Rosenbluth M.N. 1978 *Phys. Rev. Lett.* **40** 38
[32] Finken K.H. *et al* 2007 *Phys. Rev. Lett.* **98** 065001
[33] Evans T.E. *et al* 1992 *J. Nucl. Mater.* **196–198** 421
[34] Schmitz O. *et al* 2009 *J. Nucl. Mater.* **390–391** 330–34
[35] Park J.-K. *et al* 2007 *Phys. Plasmas* **14** 052110
[36] Park J.-K. *et al* 2009 *Phys. Plasmas* **16** 056115
[37] Park J.-K. *et al* 2009 *Phys. Rev. Lett.* **102** 065002
[38] Hirooka Y. *et al* 2006 *Nucl. Fusion* **46** S56
[39] Tabares F.L. *et al* 2008 *Plasma Phys. Control. Fusion* **50** 124051
[40] Paul S. *et al* 2009 *J. Nucl. Mater.* **390–391** 211
[41] Becoulet M. *et al* 2004 *J. Nucl. Mater.* **337–339** 677
[42] Kaye S. *et al* 1997 *Nucl. Fusion* **37** 1303
[43] Gates D.A. *et al* 2007 *Nucl. Fusion* **47** 1376
[44] Degeling A.W. *et al* 2003 *Plasma Phys. Control. Fusion* **45** 1637
[45] Takahashi H. *et al* 2008 *Phys. Rev. Lett.* **100** 205001
[46] Evans T.E. *et al* 2009 *J. Nucl. Mater.* **390–391** 789